

AniFaceDiff: High-Fidelity Face Reenactment via Facial Parametric Conditioned Diffusion Models

Ken Chen¹, Sachith Seneviratne¹, Wei Wang¹, Dongting Hu¹, Sanjay Saha², Md. Tarek Hasan³

Sanka Rasnayaka², Tamasha Malepathirana¹, Mingming Gong¹, and Saman Halgamuge¹

¹University of Melbourne ²National University of Singapore ³United International University

kenchen1@student.unimelb.edu.au

Abstract

Face reenactment refers to the process of transferring the pose and facial expressions from a reference (driving) video onto a static facial (source) image while maintaining the original identity of the source image. Previous research in this domain has made significant progress by training controllable deep generative models to generate faces based on specific identity, pose and expression conditions. However, the mechanisms used in these methods to control pose and expression often inadvertently introduce identity information from the driving video, while also causing a loss of expression-related details. This paper proposes a new method based on Stable Diffusion [1], called AniFaceDiff, incorporating a new conditioning module for high-fidelity face reenactment. First, we propose an enhanced 2D facial snapshot conditioning approach by facial shape alignment to prevent the inclusion of identity information from the driving video. Then, we introduce an expression adapter conditioning mechanism to address the potential loss of expression-related information. Our approach effectively preserves pose and expression fidelity from the driving video while retaining the identity and fine details of the source image. Through experiments on the VoxCeleb dataset [2], we demonstrate that our method achieves state-of-the-art results in face reenactment, showcasing superior image quality, identity preservation, and expression accuracy, especially for cross-identity scenarios. Considering the ethical concerns surrounding potential misuse, we analyze the implications of our method, evaluate current state-of-the-art deepfake detectors, and identify their shortcomings to guide future research.

1 Introduction

Face reenactment produces a video of a person engaged in conversation by transferring expressions and poses from a reference (driving) video to a source image. This technique finds applications in various fields, including film production, the video game industry, and video conferencing. Two crucial objectives define this task: 1) preserving the identity and background details of the source image; and 2) transferring pose and expression from the driving video onto the static source image. However, achieving a faithful generation that fulfills these criteria remains a significant challenge.

The advancement of deep generative models, including Generative Adversarial Networks (GANs) [3] and diffusion models [4], has facilitated the successful deployment of convenient and high-quality face reenactment techniques. A typical line of the state-of-the-art GANs or diffusion models based methods [5, 6, 7, 8] relies on flow fields to complete the transferring of the pose and the expression. Initially, keypoints of the source image and the driving video are extracted in an unsupervised manner, followed by the estimation of motion flow fields based on these keypoints to capture pose and expression changes. These flow fields are then utilized to warp either the source image or its features. However, the incorporation of estimated flow fields inadvertently introduces identity information from the driving video onto the source image, resulting in a subpar performance in cases of identity mismatch between the source image and the driving video [9]. Moreover, flow fields often cause distortions, particularly in situations involving significant pose and expression variations between the source image and the driving video.

More recent research on face reenactment has highlighted the potential of pretrained 3D parametric face models [10, 11, 12], for representing the semantic meaning of human faces, including expressions, poses, and identities. Methods based on StyleGAN [13], e.g., StyleHeat [14] and HyperReenact [15], utilize parameters or feature maps from 3D face models to adjust the feature map or weights of GAN-generators. However, these approaches are limited by their reliance on finding a latent representation of the source image within the StyleGAN space that can be manipulated. This often leads to inadequate reconstruction

of the source image, including both identity information and background details. Diffusion models have also been extended alongside 3D face models [16, 17] owing to their remarkable performance. However, the conditioning mechanisms of these methods still introduce unexpected identity-related information due to the direct use of the driving image to generate the condition. Furthermore, the typically low resolution of 3D face meshes leads to the loss of necessary expression-related information, particularly mid-frequency details [12].

In this work, we propose a method named AniFaceDiff, for face reenactment by incorporating conditional signals to the pretrained text-to-image Stable Diffusion model [1], as shown in Fig. 1. We introduce a new conditioning mechanism to address the limitations of previous methods. Specifically, 1) to avoid introducing unexpected identity-related information from the driving image, we propose a Facial Shape Alignment (FSA) strategy to form spatial-aligned conditions for the diffusion models. This involves extracting pose and expression parameters from the driving video and shape parameters from the source image using the 3D face model (DECA [12]), and then generating 2D face surface normal snapshots with these facial parameters. 2) To mitigate potential expression-related information loss, we introduce an Expression Adapter (EA) that injects the expression embedding into the cross-attention layers of the denoising UNet [18]. This adapter compensates for the information loss in spatial-aligned conditions, thereby enhancing expression fidelity.

In summary, our main contributions are:

- 1) We propose a face reenactment framework, AniFaceDiff, based on diffusion models with accurate conditioning. Our approach effectively preserves pose and expression fidelity from the driving video simultaneously retaining the identity and background details of the source image in a one-shot setting (solely utilizing a single source image).
- 2) We design a new conditioning mechanism based on 3D face model, which furnishes both accurate spatial and non-spatial conditions for diffusion models, thereby facilitating faithful reenactment.
- 3) Experiments on the VoxCeleb [2] benchmark demonstrate that our method achieves state-of-the-art performance in face reenactment tasks. Furthermore, our method has robust generalization capabilities, even when applied to out-of-domain data.

2 Related Work

Neural face reenactment

The development of deep generative models has facilitated convenient and high-quality face reenactment applications. A prevalent approach involves warping the source image or latent representation using deformation fields (e.g., optical flow fields) to convey pose and transfer expressions [21, 22, 5, 6, 9, 7, 23, 24, 25, 26, 27, 8]. For instance, Monkey-Net [22] employs a motion transfer network alongside unsupervised keypoint detection and dense motion prediction to generate animated frames. FOMM [5] enhances Monkey-Net by incorporating motion field computation with a first-order Taylor expansion approximation, encompassing keypoints and affine transformations. Face vid2vid [6] extends FOMM for free-view talking face video generation utilizing a free-view keypoints representation. TPSMM [7] introduces thin-plate spline motion estimation to generate a more flexible optical flow. However, optical flow fields are susceptible to introducing artifacts and blur, especially in instances of large identity or pose mismatches between the source image and driving video. To mitigate this issue, MRAA [9] proposes an Animation Via Disentanglement (AVD) network to separate the control of shape and pose. However, improvements in results are not as significant for objects like faces.

Another line of research exploits the learned prior of pretrained 3D parametric face models. PIRenderer [28] utilizes the parameters of 3D morphable face models (3DMMs) to adjust intermediate results from the warping network. HeadGAN [29] generates faces with warped source features, 3d face shape and audio. StyleHeat [14], based on StyleGAN [13], integrates 3DMMs with StyleGAN by predicting flow fields with 3DMM parameters and warping the feature map from the encoder of GAN inversion. However, these methods based on 3D face models still depend on flow fields and often necessitate additional refinement to attain satisfactory results. In addition, StyleGAN-based methods rely on GAN inversion, which may struggle to achieve high-fidelity reconstruction following extensive edits [15]. HyperReenact [15] employs the feature map of the pretrained DECA encoder to update the weights of the pretrained StyleGAN generator, allowing it to perform well even under large pose variations. PASL [30] proposes pose adapted shape learning for large pose reenactment. Our method aims to enhance the accuracy of both identity preservation and expression.

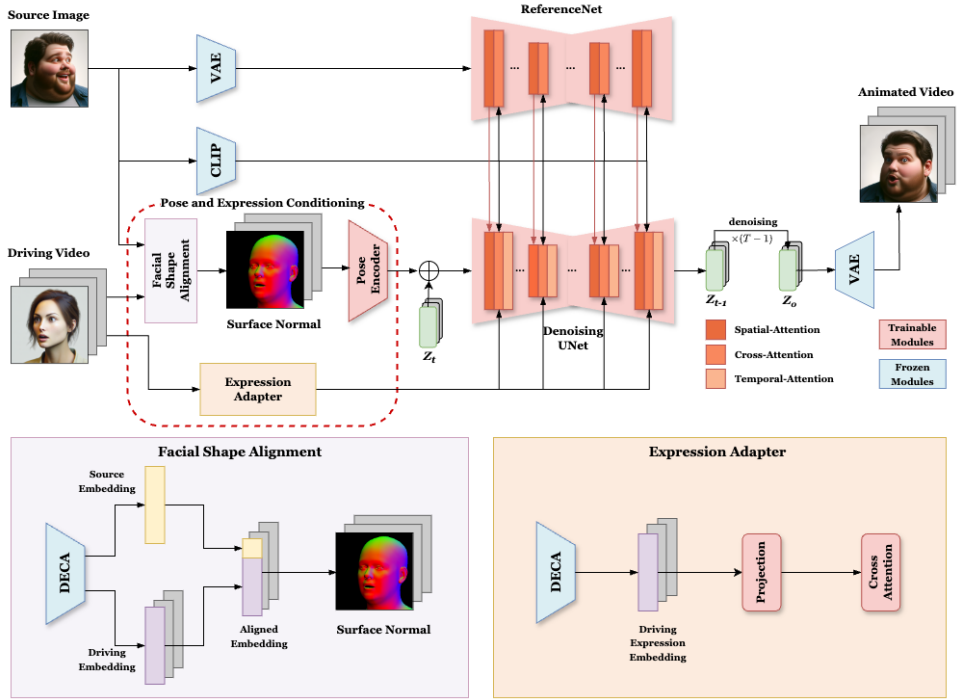


Figure 1: **The overview of the proposed method.** A VAE [19] encoder and the ReferenceNet extract detailed features from the source image, which are then merged into the Stable Diffusion backbone Denoising UNet via spatial-attention. A CLIP Image Encoder [20] extracts semantic features from the source image, which is then injected into both the ReferenceNet and the Denoising UNet via cross-attention. The pose and expression conditioning is portrayed within the red dashed box. The facial shape of the source image and the pose and expression of the driving video are extracted to form 2D surface normal facial snapshots through Facial Shape Alignment. These snapshots are then encoded and concatenated with the input of the Denoising UNet. The expression of driving frames is further injected into the cross-attention layers of the Denoising UNet by the expression adapter to improve the expression consistency. Temporal-attention aims to improve the temporal consistency across frames. After iterative denoising, the output of the Denoising UNet is decoded into the final animated video by a VAE decoder.

Image generation with diffusion models

Diffusion models have achieved success across various tasks including unconditional image generation [4, 31, 32], image super-resolution [32], text-to-image generation [33], image-to-image translation [34] and even video generation [35, 36, 37, 38]. Diffusion models possess the capability to capture the full distribution of datasets, making them increasingly popular compared to GANs in recent years. The iterative refinement process also results in the production of diverse and high-quality generated images. Stable Diffusion [1] extends diffusion models into the latent space to significantly reduce computational costs and achieve superior results compared to those in the pixel space.

Conditioning serves as a crucial element in maximizing the potent generative capabilities for various downstream tasks, enabling controllable generation [39, 40, 16, 17, 41, 42, 43]. The two primary conditioning mechanisms for diffusion models involve concatenation and cross-attention [1]. Liu et al. [44] propose an alternative intuitive approach based on [32] and a CLIP-based encoder for semantic diffusion guidance in both text and image conditioning. ControlNet [45] is extensively utilized for spatial-aligned conditioning by updating each layer of the Stable Diffusion backbone UNet via trainable copy and zero convolution layers. IP-adapter [46] integrates image conditions into pretrained text-to-image diffusion models using a decoupled cross-attention mechanism. Our pose and expression conditioning module employs designs similar to those of ControlNet and IP-adapter.

Human image animation with diffusion models

Animating a static image into a temporally consistent video [47, 48, 49, 50, 51] has garnered significant attention among researchers. In human image animation, DisCo [52] introduces human appearance conditioning to Stable Diffusion using a CLIP image encoder and separate ControlNets for background and pose conditions to generate human dancing videos. Animate Anyone [53] employs spatial attention and a ReferenceNet, a copy of UNet, to incorporate detailed information into Stable Diffusion and demonstrate its generalization capability. Champ [54] enhances previous approaches by utilizing a 3D human parametric model with multiple pose conditions. In audio-driven talking head generation, EMO [55] proposes a direct audio-to-video framework leveraging pretrained wave2vec [56]. VLOGGER [57] predicts face and body parameters from audio to render dense masks as conditions for generating talking avatars. We are inspired by previous efforts utilizing the ReferenceNet and spatial-aligned pose conditions due to the similarity of the task. We focus on achieving accurate face reenactment guided by pose and expression while minimizing the impact of identity mismatches.

3 Method

Our method is designed for one-shot face reenactment, which involves generating a realistic video based on the guidance of a single source image and a driving video. The framework of the proposed method is illustrated in Fig. 1. First, we give a brief introduction of the foundational model – Stable Diffusion and the 3D face model (Sec.3.1). Second, we introduce the overall structure of the framework (Sec.3.2). Then, we detail the proposed pose and expression conditioning mechanism (Sec.3.3). Finally, we illustrate the detailed information of training and inference in Sec.3.4

3.1 Preliminaries

Stable Diffusion. Denoising Diffusion Probabilistic Models (DDPM) [4] are a class of generative models that operates by simulating data through the introduction of noise and subsequently denoising it in a progressive manner to generate samples representative of the true data distribution. This step-by-step noising and denoising process endows the model with the ability to generate high-quality images. However, it comes with a high computational resource requirement.

To address this challenge, Stable Diffusion [1] conducts the noising and denoising process in a latent space rather than the pixel space. This enables considerable computational cost savings. The high efficiency allows Stable Diffusion to be pretrained on extremely large-scale datasets (e.g. LAION-5B [58]). Specifically, Stable Diffusion utilizes a pretrained autoencoder to encode the given image \mathbf{x}_0 into a latent representation \mathbf{z}_0 using the encoder. Subsequently, the latent representation can be reconstructed into the pixel space by the decoder. In the training process, Stable Diffusion adds Gaussian noise ϵ to the latent representation \mathbf{z}_0 at each timestep t by a noise scheduler. The backbone denoising UNet is trained to predict the added noise ϵ . During the inference process, the starting point is usually a randomly selected

noise. The trained UNet is utilized to predict the noise under the text condition at each timestep and subsequently conducts the denoising process step by step until a clean image is generated.

3D morphable face models (3DMMs). 3DMMs are parametric models designed to accurately represent facial shape and expression. These models are constructed using dimensionality reduction techniques such as principal component analysis (PCA) and are capable of reconstructing 3D faces based on 2D images. FLAME [11] is a notable example of a 3DMM that relies on standard vertex-based linear blend skinning with blendshapes to generate a mesh with 5023 vertices, which is formulated as:

$$M(\beta, \theta, \psi) = W(T_p(\beta, \theta, \psi), \mathbf{J}(\beta), \theta, \mathcal{W}) \quad (1)$$

where β , θ , and ψ represent parameters of identity, pose, and expression, respectively. W is the blend skinning function that rotates the vertices in T_p around joints \mathbf{J} smoothed by blendweights \mathcal{W} . Detailed information can be found in FLAME [11]. In this paper, we utilize the widely used 3D face model DECA [12] which is capable of estimating parameters, including those of the FLAME model, from a single image. This allows for the reconstruction of a 3D face with detailed facial geometry.

3.2 Framework Architecture

In this section, we illustrate the overall framework of our method, which takes a source image and a driving video as inputs and outputs a reenacted video. We formulate face reenactment as conditional generation, where all the identity, pose, and expression of the generated content are controllable via the corresponding conditioning mechanism. Our method is based on the pretrained Stable Diffusion 1.5 and follows a similar structure to the backbone denoising UNet. First, the source image is encoded into a latent space using a VAE encoder, and its features are extracted by a **ReferenceNet**. Second, we utilize a CLIP image encoder to extract semantic information, which is crucial for preserving the identity of the source image. This semantic information is injected into the ReferenceNet and Denoising UNet via cross-attention. To effectively introduce pose and expression, we propose a pose and expression conditioning module as elaborated in 3.3. Furthermore, we employ **Temporal Modules** to generate temporally consistent content as we detail below. The diffusion model performs iterative denoising on the latent space and finally transforms the denoised output back to the pixel space through a VAE decoder to get the generated video.

ReferenceNet. ReferenceNet is a copy of the backbone denoising UNet (without temporal modules) used to extract features at multiple resolutions containing the face and background of the source image. It has been widely utilized [53, 55, 54] to improve the appearance consistency between the reference and the output. These features are then merged into the denoising UNet using a spatial-attention mechanism similar to Animate Anyone [53]. Specifically, the output of each self-attention layer of ReferenceNet ($z_1 \in \mathbb{R}^{b \times c \times h \times w}$) is repeated f times (the length of the video clip) and concatenated with that of the denoising UNet ($z_2 \in \mathbb{R}^{b \times c \times f \times h \times w}$). The model then applies self-attention on the concatenated output ($z_{concat} \in \mathbb{R}^{b \times c \times f \times h \times 2w}$) and takes the first half of the feature map as the final output ($z_{out} \in \mathbb{R}^{b \times c \times f \times h \times w}$).

Temporal Module. We employ temporal modules similar to AnimateDiff [59] to improve the temporal consistency across the generated frames. Specifically, the feature map of 3D denoising UNet $z \in \mathbb{R}^{b \times c \times f \times h \times w}$ is firstly reshaped as $z \in \mathbb{R}^{(b \times h \times w) \times f \times c}$. The reshaped feature map is then operated with temporal-attention, which consists of several self-attention blocks along the frame dimension f . The temporal module is inserted after the cross-attention layer of each resolution level of denoising UNet via a residual connection.

3.3 Pose and Expression Conditioning

Our pose and expression conditioning module extracts pose and expression from the driving video, and identity-related information from the source image based on a pretrained off-the-shelf 3D face model, DECA. Subsequently, we condition the diffusion model using two components: improved spatial conditioning and non-spatial conditioning (the expression adapter).

Improved Spatial Conditioning with Facial Shape Alignment

We utilize the encoder of DECA to estimate facial parameters from each frame of the driving video directly. Subsequently, we render these parameters into a sequence of 2D facial surface normal snapshots. However, in addition to containing the pose and expression information we require, these snapshots

also include identity information reflected by the facial geometry from the driving frames. The identity information essential for our purpose should be extracted from the source image. Any inconsistency in the facial geometry information between the condition and the final output can result in sub-optimal performance, particularly noticeable when there is a significant mismatch in identity between the source image and the driving video. To address this issue, we utilize a facial shape alignment strategy which combines the identity information from the source image with the pose and expression information from the driving frames to generate the refined 2D facial conditions.

Specifically, we obtain shape parameters β containing identity information from the source image, and other parameters including pose θ and expression ψ from the driving frames by the DECA encoder. We then use FLAME to generate the 3D face meshes and render them into surface normal snapshots to eliminate the effects of lighting conditions. The entire process can be represented as:

$$n^{1:N} = \mathcal{R}(M(\beta_s, \theta_d^{1:N}, \psi_d^{1:N}), c_d^{1:N}), \quad (2)$$

where $n^{1:N}$ represents the 2D facial conditions, the rendered surface normal snapshots, for frames $1 : N$. \mathcal{R} represents the rasterizer (PyTorch3D [60]). M represents FLAME model used to obtain head vertices with facial parameters. c represents the camera information to project the 3D mesh into image space. β_s is extracted from the source image, while $\theta_d^{1:N}$, $\psi_d^{1:N}$ and $c_d^{1:N}$ are extracted from the driving frames.

After extracting the 2D facial conditions which are spatial-aligned with the output frames, we encode them with the Pose Encoder, a series of convolution layers, similar to Animate Anyone [53], to project the conditions to the same resolution with the noisy input of denoising UNet. Subsequently, we concatenate the spatial-aligned condition with the noisy input and feed it to the denoising UNet.

Expression Adapter

Crucially, the low resolution of the 3D face mesh leads to the loss of mid-frequency details related to expression. Drawing inspiration from IP-Adapter [46] for image prompt conditioning, we introduce an expression adapter conditioning mechanism to address potential information loss resulting from spatial modulation, as illustrated in the lower branch of Fig. 1. Unlike IP-Adapter for conditional image generation, we integrate video-level expression prompts from the driving frames in parallel with the image prompt from the source image. Specifically, we extract the expression embedding $\psi \in \mathbb{R}^{N \times 50}$ from N driving frames using DECA and project it into the same dimension as the CLIP image embedding. This projected expression embedding p_ψ is then injected into the diffusion model through additional cross-attention layers, which can be represented as:

$$Z_{new} = Attention(Q, K^i, V^i) + \lambda \cdot Attention(Q, K^\psi, V^\psi), \quad (3)$$

where Q , K^i , and V^i are the query, key, and value matrices from the original cross-attention layer for CLIP image features, while K^ψ and V^ψ are from the additional cross-attention layer for expression features. The projected expression embedding p_ψ is injected into the cross-attention layer as $K^\psi = p_\psi W_k^\psi$ and $V^\psi = p_\psi W_v^\psi$, where W_k^ψ and W_v^ψ are the corresponding weight matrices. In the 3D denoising UNet for generating a video, the CLIP embedding of the source image is repeated N times to match the length of the expression embedding from the driving frames.

3.4 Training and Inference

The training process comprises two stages. In the first stage, the model is trained to generate a single image under the guidance of a source image and a driving frame. During the training process, the model utilizes same-identity construction as its objective, where both the source image and the driving frame are derived from the same video. DECA is utilized to extract facial parameters and render facial snapshots from the driving frame. The driving frame \mathbf{x}_0 is first encoded into the latent representation \mathbf{z}_0 , which is then noised with $\epsilon \sim \mathcal{N}(0, 1)$ at timestep t via a defined scheduler as:

$$\mathbf{z}_t = \sqrt{\bar{\alpha}_t} \mathbf{z}_0 + \sqrt{1 - \bar{\alpha}_t} \epsilon \quad (4)$$

where $\bar{\alpha}_t = \prod_{s=0}^t \alpha_s$, α_t is the variance schedule, and \mathbf{z}_t is the noisy latent. The model is trained to predict the added noise by denoising function ϵ_θ with condition features \mathbf{f} from the source image and the driving video. The VAE, CLIP image encoder, and DECA are pretrained and kept frozen while the pose

encoder, the expression adapter, the ReferenceNet, and the denoising UNet are updated. The training objective of the first stage is similar to that of Stable Diffusion [1]:

$$\mathbf{L}_{stage1} = \mathbb{E}_{t, \mathbf{f}, \epsilon, \mathbf{z}_t} [\|\epsilon - \epsilon_\theta(\mathbf{z}_t, t, \mathbf{f})\|_2^2] \quad (5)$$

In the second stage, the models are trained to generate a temporally consistent video clip (N frames) with guidance from both a source image and a driving video clip. Pretrained temporal modules [59] are integrated into the denoising UNet. During this stage, only the temporal modules are updated and all other components remain frozen. The training objective of the second stage is formulated as:

$$\mathbf{L}_{stage2} = \mathbb{E}_{t, \mathbf{f}^{1:N}, \epsilon, \mathbf{z}_t^{1:N}} [\|\epsilon - \epsilon_\theta(\mathbf{z}_t^{1:N}, t, \mathbf{f}^{1:N})\|_2^2] \quad (6)$$

At inference, we utilize DECA to extract information from both the source image and the driving video. Leveraging a facial shape alignment strategy, we refine the facial snapshot sequence. Beginning with noises $\mathbf{z}_t^{1:N}$ sampled from a Gaussian distribution in the latent space, the model conduct denoising process to $\mathbf{z}_{t-1}^{1:N}$ by predicting noise using the denoising UNet with the condition $\mathbf{f}^{1:N}$ and iteratively to $\mathbf{z}_0^{1:N}$ via a defined sampling process. Finally, the denoised outputs $\mathbf{z}_0^{1:N}$ are projected back to the pixel level $\mathbf{x}_0^{1:N}$ to obtain the generated video via the VAE decoder.

4 Experiments

In our experiments, we utilized the VoxCeleb dataset [2] after preprocessing as described in [5]. This dataset comprises 19,522 and 525 utterance sequences, spanning 453 and 13 identities, with 3,354 and 90 videos in the training and test sets, respectively.

Training was conducted on 256×256 images using 2 NVIDIA A100 GPUs. In the first stage, we trained for over 100,000 steps with a batch size of 32. Subsequently, in the second stage, we trained for over 20,000 steps using a batch size of 8 for a video clip consisting of 24 frames. All models were optimized using the Adam optimizer with a learning rate of 1×10^{-5} .

4.1 Comparisons

We compare our method with four state-of-the-art methods, namely FOMM [5], Face vid2vid [6], TPSMM [7], and HyperReenact [15]. Results for the baseline methods are generated using their provided code and pretrained weights, with the exception of Face vid2vid, for which we utilize unofficial code¹ due to the absence of the official version. We assess our method and the baseline approaches using four distinct metrics. First, we utilize the Fréchet-Inception Distance (FID) to evaluate image quality by measuring the distribution discrepancy between the generated data and the test set of VoxCeleb. Second, we employ the identity preservation cosine similarity (CSIM), following the approach outlined in Encoding in Style [61], to quantify the preservation of identity. Third, we measure the accuracy of pose and expression transfer using the Average Pose Distance (APD) and the Average Expression Distance (AED). CSIM is computed based on the source image and the outputs, while APD and AED are calculated based on the driving video and the outputs.

Quantitative Comparisons

We evaluate our method and the baselines on the test set of VoxCeleb. In the evaluation, higher scores indicate better performance for CSIM, while lower scores are preferable for all other metrics. We conduct one-shot face reenactment on two tasks: same-identity reconstruction, which mirrors the training process, and the more challenging primary task of cross-identity reenactment.

For the same-identity reconstruction task, we randomly selected 100 videos from the VoxCeleb test set, using the first frame as the source image and considering the remaining frames as the driving frames. As shown in Table 1, our method achieves the best image quality (FID) and ranks second for pose (APD) and expression accuracy (AED). TPSMM outperforms all other methods in terms of CSIM, APD, and AED. All warping-based methods (FOMM, Face vid2vid, and TPSMM) perform well on this proxy task when there is no identity variance and usually a small pose difference between the source image and the driving video.

¹https://github.com/zhanglonghao1992/One-Shot_Free-View_Neural_Talking_Head_Synthesis

Table 1: Quantitative results on VoxCeleb. The best results are shown in **bold**, and the second-best results are shown in underline

	Same-identity Reconstruction				Cross-identity Reenactment				User Pref. (%)
	FID↓	CSIM↑	APD↓	AED↓	FID↓	CSIM↑	APD↓	AED↓	
FOMM [5]	21.91	0.83	<u>0.011</u>	0.092	41.93	0.51	0.028	0.210	10.25
Face vide2vid [6]	<u>18.57</u>	0.84	0.012	0.092	<u>35.21</u>	<u>0.56</u>	0.034	0.238	9.50
TPSMM [7]	20.18	0.84	0.009	0.081	38.91	0.52	0.024	0.191	16.50
HyperReenact [15]	72.72	0.48	<u>0.011</u>	0.098	73.35	0.40	0.017	<u>0.181</u>	<u>20.75</u>
Ours	17.21	0.75	<u>0.011</u>	<u>0.091</u>	32.58	0.57	<u>0.022</u>	0.174	43.00

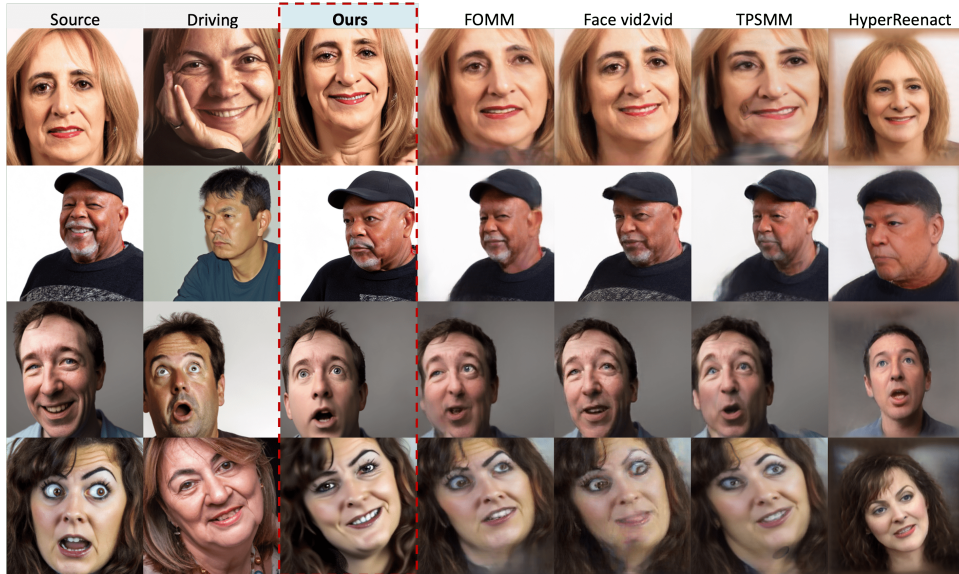


Figure 2: Qualitative comparison with SOTA methods on cross-identity reenactment. Our method achieves high identity preservation and expression accuracy. (All photorealistic human images presented in this paper are virtual individuals generated by [33] and do not exist in the real world.)

Even though current methods perform well on same-identity reconstruction, the main task (cross-identity reenactment), where the source image and driving video are from different identities, introduces substantial identity mismatches and pose variations, demanding higher generalization capabilities from models. Similar to previous work, we randomly select 100 image-video pairs from the VoxCeleb test set. Table.1 illustrates a significant performance drop for each method when transitioning from same-identity reconstruction to cross-identity reenactment. As observed in previous SOTA methods, there is a trade-off between identity consistency (CSIM) and expression accuracy (AED). The more modifications related to expression made to the original source identity, the less the generated image will resemble the original, as assessed by face recognition models. Despite this trade-off, Our method (AniFaceDiff) achieves SOTA results on both CSIM and AED. Additionally, we outperform all four baseline methods in terms of image quality (FID) and secure the second position in terms of pose accuracy (APD).

Qualitative Comparisons

We present a few representative examples of cross-identity reenactment in Fig. 2. Additional examples can be found in Appendix A.2. Overall, our method generates high quality images compared to all other state-of-the-art methods while preserving both source identity and pose and expression of the driving frame. Better preservation of source identity is especially evident in the first and second rows, where other methods show noticeable influence from the driving identity. In contrast, our method maintains the source identity with greater accuracy. Furthermore, our approach excels at maintaining the expressions and poses of the driving videos, as seen in the third and fourth rows, where our method consistently captures expression-related details such as wrinkles, brow furrows and lip curvature more accurately than



Figure 3: Qualitative comparison with SOTA methods on cross-identity reenactment in the presence of significant pose variations between the source and driving images. Our method accurately captures the source identity and faithfully transfers the target pose and expression, even under significant pose variations.

other state-of-the-art methods.

Fig.3 demonstrates a more challenging scenario where there are significant pose differences between the source and driving images. FOMM, Face vid2vid, and TPSMM tend to produce blurry outputs with severe artifacts and distortions due to their reliance on the optical flow field. Additionally, their inadequate inpainting capabilities result in blurry and unrealistic regions when generating areas not present in the source image. HyperReenact, which does not rely on the optical flow field, generates more fine-grained results. However, it still suffers from a loss of identity and detailed information, such as facial wrinkles, hair texture, and lighting. This is likely due to the limitations of GAN inversion and the use of a pretrained ArcFace [62] for extracting identity information from the source image. In contrast, our method excels in preserving detailed information from the source image, while accurately maintaining pose and expression from the driving video due to the designed conditioning module. Overall, our method produces the cleanest and most high-fidelity results among all the state-of-the-art methods, even when the source face is partially occluded (row 3) or when there is a large distance difference from the camera between the source and driving images (row 4).

We note that the current metrics might not fully capture the qualitative differences observed in the results. Hence, we conducted a user study involving 20 participants to further assess performance based on human visual experience. We presented 20 randomly selected source-driving image pairs: 5 for same-identity reconstruction and 15 for cross-identity reenactment, as cross-identity reenactment is the primary task. We provided users with three evaluation criteria similar to those used by HyperReenact [15]: 1) image quality, 2) identity and nuanced detail preservation from the source image, and 3) pose and expression preservation from the driving image. As shown in Table 1, our method significantly outperforms all other SOTA methods based on user preference.

Out-of-domain Data

We also compare our method with these SOTA methods outside the training distribution to evaluate generalization capabilities. As shown in Fig. 4, The first and second rows demonstrate out-of-domain (non-photorealistic) source images reenacted by out-of-domain driving images. The third and fourth rows demonstrate out-of-domain source images reenacted by in-domain (photorealistic) driving images. Our method exhibits strong generalization capabilities on out-of-domain data. More results can be found in Appendix A.3.

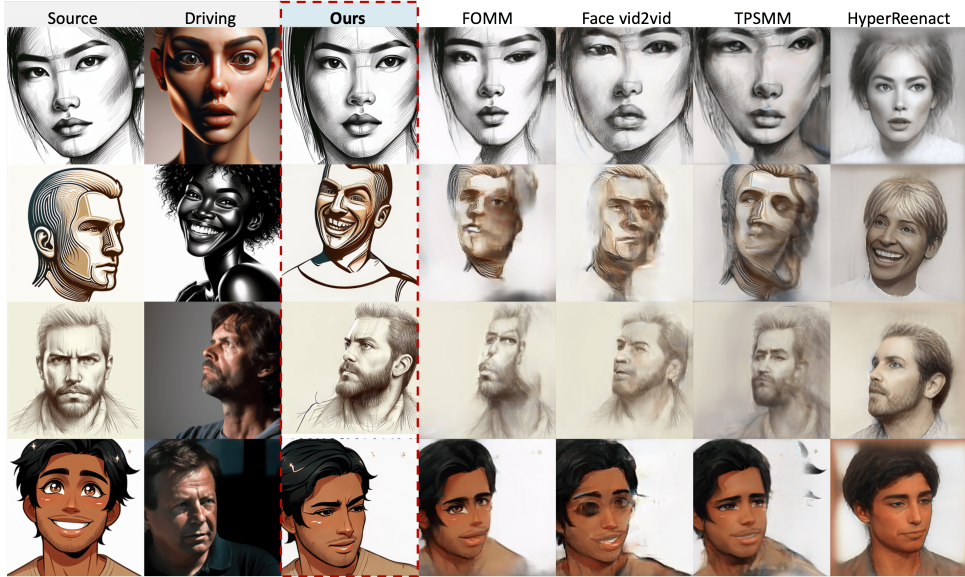


Figure 4: Qualitative comparison with SOTA methods on out-of-domain (non-photorealistic) face reenactment. Our method can generate high-quality images even without being trained on such types of data. (All out-of-domain facial images are generated by [63])

Table 2: Quantitative comparison with or without Facial Shape Alignment and the Expression Adapter. The addition of both components allows for a better trade-off between identity consistency vs expression fidelity. We find that combining both provides the best qualitative and quantitative results.

		Same-identity Reconstruction			Cross-identity Reenactment		
<i>FSA</i>	<i>EA</i>	CSIM \uparrow	APD \downarrow	AED \downarrow	CSIM \uparrow	APD \downarrow	AED \downarrow
-	-	0.75	0.011	0.098	0.52	0.021	0.182
\checkmark	-	-	-	-	0.59	0.022	0.206
-	\checkmark	0.75	0.011	0.091	0.51	0.021	0.158
\checkmark	\checkmark	-	-	-	0.57	0.022	0.174



Figure 5: Qualitative comparison on cross-identity reenactment with or without Facial Shape Alignment and the Expression Adapter. FSA improves facial generation quality, while EA maintains expression consistency. Ensembling both provides the best overall consistency. These observations are consistent with the quantitative results in Table 2.

4.2 Ablation Study

We conduct an ablation study on the proposed 1) Facial Shape Alignment (FSA) and 2) Expression Adapter (EA). Facial Shape Alignment is used exclusively for cross-identity reenactment. Our baseline method directly conditions the model with 2D facial snapshots extracted from the driving video, without the facial

shape alignment and the expression adapter. As illustrated in Table 2, adding facial shape alignment significantly improves identity preservation (CSIM). Facial shape alignment uses the shape embedding from the source image to render the 2D facial snapshots, thereby enhancing identity preservation. Without facial shape alignment, the output maintains the shape from the driving image rather than the source image, as shown in Fig. 5. The expression adapter significantly enhances expression accuracy (AED) in both same-identity reconstruction and cross-identity reenactment. Methods incorporating the expression adapter can provide more expression-related details, such as wrinkles, and achieve greater accuracy in certain areas, such as the mouth, as depicted in Fig. 5. Combining both FSA and EA can effectively handle the trade-off between identity consistency and expression accuracy.

5 Ethical Considerations

We are committed to positive virtual face reenactment applications. All photorealistic human portraits presented in this paper are virtual and do not exist in reality. Acknowledging the broad applicability of face reenactment, we are also aware of its potential for malicious misuse, such as in deepfake fraud. To address this concern, we plan to implement stringent access control mechanisms to limit access permissions exclusively for research purposes. Additionally, we evaluate existing SOTA deepfake detectors (see Appendix A.1) and conduct an analysis to identify potential shortcomings. This will serve as a foundation for future research aimed at mitigating weaknesses of existing detectors and providing benchmarking data for future approaches.

References

- [1] R. Rombach, A. Blattmann, D. Lorenz, P. Esser, and B. Ommer, “High-resolution image synthesis with latent diffusion models,” pp. 10 684–10 695, Dec. 2021.
- [2] A. Nagrani, J. S. Chung, and A. Zisserman, “VoxCeleb: a large-scale speaker identification dataset,” Jun. 2017.
- [3] I. Goodfellow, J. Pouget-Abadie, and others, “Generative adversarial nets,” *Adv. Neural Inf. Process. Syst.*, 2014.
- [4] J. Ho, A. Jain, and P. Abbeel, “Denoising diffusion probabilistic models,” pp. 6840–6851, Jun. 2020.
- [5] A. Siarohin, S. Lathuilière, S. Tulyakov, and others, “First order motion model for image animation,” *Adv. Neural Inf. Process. Syst.*, 2019.
- [6] T.-C. Wang, A. Mallya, and M.-Y. Liu, “One-shot free-view neural talking-head synthesis for video conferencing,” pp. 10 039–10 049, Nov. 2020.
- [7] J. Zhao and H. Zhang, “Thin-plate spline motion model for image animation,” pp. 3657–3666, Mar. 2022.
- [8] B. Zeng, X. Liu, S. Gao, B. Liu, H. Li, J. Liu, and B. Zhang, “Face animation with an Attribute-Guided diffusion model,” Apr. 2023.
- [9] J. Ren, M. Chai, and S. Tulyakov, “Motion representations for articulated animation,” *Proceedings of the*, 2021.
- [10] V. Blanz and T. Vetter, “A morphable model for the synthesis of 3d faces,” in *Seminal Graphics Papers: Pushing the Boundaries, Volume 2*, 2023, pp. 157–164.
- [11] T. Li, T. Bolkart, M. J. Black, H. Li, and J. Romero, “Learning a model of facial shape and expression from 4D scans,” *ACM Trans. Graph.*, vol. 36, no. 6, pp. 1–17, Dec. 2017.
- [12] Y. Feng, H. Feng, M. J. Black, and T. Bolkart, “Learning an animatable detailed 3D face model from in-the-wild images,” *ACM Trans. Graph.*, vol. 40, no. 4, pp. 1–13, Jul. 2021.
- [13] T. Karras, S. Laine, and T. Aila, “A Style-Based generator architecture for generative adversarial networks,” *IEEE Trans. Pattern Anal. Mach. Intell.*, vol. 43, no. 12, pp. 4217–4228, Dec. 2021.

- [14] F. Yin, Y. Zhang, X. Cun, M. Cao, Y. Fan, X. Wang, Q. Bai, B. Wu, J. Wang, and Y. Yang, “StyleHEAT: One-Shot High-Resolution editable talking face generation via pre-trained StyleGAN,” in *Computer Vision – ECCV 2022*. Springer Nature Switzerland, 2022, pp. 85–101.
- [15] S. Bounareli, C. Tzelepis, V. Argyriou, I. Patras, and G. Tzimiropoulos, “Hyperreenact: one-shot reenactment via jointly learning to refine and retarget faces,” in *Proceedings of the IEEE/CVF International Conference on Computer Vision*, 2023, pp. 7149–7159.
- [16] Z. Ding, X. Zhang, Z. Xia, L. Jebe, Z. Tu, and X. Zhang, “Diffusionrig: Learning personalized priors for facial appearance editing,” in *Proceedings of the IEEE/CVF Conference on Computer Vision and Pattern Recognition*, 2023, pp. 12 736–12 746.
- [17] H. Jia, Y. Li, H. Cui, D. Xu, C. Yang, Y. Wang, and T. Yu, “DisControlFace: Disentangled control for personalized facial image editing,” Dec. 2023.
- [18] O. Ronneberger, P. Fischer, and T. Brox, “U-net: Convolutional networks for biomedical image segmentation,” in *Medical image computing and computer-assisted intervention–MICCAI 2015: 18th international conference, Munich, Germany, October 5-9, 2015, proceedings, part III 18*. Springer, 2015, pp. 234–241.
- [19] D. P. Kingma and M. Welling, “Auto-encoding variational bayes,” *arXiv preprint arXiv:1312.6114*, 2013.
- [20] A. Radford, J. W. Kim, C. Hallacy, A. Ramesh, G. Goh, S. Agarwal, G. Sastry, A. Askell, P. Mishkin, J. Clark, G. Krueger, and I. Sutskever, “Learning transferable visual models from natural language supervision,” in *Proceedings of the 38th International Conference on Machine Learning*, ser. Proceedings of Machine Learning Research, M. Meila and T. Zhang, Eds., vol. 139. PMLR, 2021, pp. 8748–8763.
- [21] O. Wiles, A. Koepke, and A. Zisserman, “X2face: A network for controlling face generation using images, audio, and pose codes,” in *Proceedings of the European conference on computer vision (ECCV)*, 2018, pp. 670–686.
- [22] A. Siarohin, S. Lathuiliere, S. Tulyakov, E. Ricci, and N. Sebe, “Animating arbitrary objects via deep motion transfer,” in *2019 IEEE/CVF Conference on Computer Vision and Pattern Recognition (CVPR)*. IEEE, Jun. 2019, pp. 2377–2386.
- [23] C. Xu, J. Zhang, Y. Han, G. Tian, X. Zeng, Y. Tai, Y. Wang, C. Wang, and Y. Liu, “Designing one unified framework for High-Fidelity face reenactment and swapping,” in *Computer Vision – ECCV 2022*. Springer Nature Switzerland, 2022, pp. 54–71.
- [24] W. Li, L. Zhang, D. Wang, B. Zhao, Z. Wang, M. Chen, B. Zhang, Z. Wang, L. Bo, and X. Li, “One-shot high-fidelity talking-head synthesis with deformable neural radiance field,” pp. 17 969–17 978, Apr. 2023.
- [25] Y. Wang, D. Yang, F. Bremond, and A. Dantcheva, “Latent image animator: Learning to animate images via latent space navigation,” *arXiv preprint arXiv:2203.09043*, 2022.
- [26] Y. Wang, X. Ma, X. Chen, A. Dantcheva, B. Dai, and Y. Qiao, “LEO: Generative latent image animator for human video synthesis,” May 2023.
- [27] H. Ni, C. Shi, K. Li, S. X. Huang, and M. R. Min, “Conditional image-to-video generation with latent flow diffusion models,” pp. 18 444–18 455, Mar. 2023.
- [28] Y. Ren, G. Li, Y. Chen, T. H. Li, and S. Liu, “PIRenderer: Controllable portrait image generation via semantic neural rendering,” in *2021 IEEE/CVF International Conference on Computer Vision (ICCV)*. IEEE, Oct. 2021, pp. 13 759–13 768.
- [29] M. C. Doukas, S. Zafeiriou, and V. Sharmanska, “HeadGAN: One-shot neural head synthesis and editing,” pp. 14 398–14 407, Dec. 2020.
- [30] G.-S. J. Hsu, J.-Y. Zhang, H. Y. Hsiang, and W.-J. Hong, “Pose adapted shape learning for large-pose face reenactment,” in *Proceedings of the IEEE/CVF Conference on Computer Vision and Pattern Recognition*, 2024, pp. 7413–7422.

- [31] J. Song, C. Meng, and S. Ermon, “Denoising diffusion implicit models,” Oct. 2020.
- [32] P. Dhariwal and A. Nichol, “Diffusion models beat gans on image synthesis,” *Adv. Neural Inf. Process. Syst.*, vol. 34, pp. 8780–8794, 2021.
- [33] A. Ramesh, P. Dhariwal, A. Nichol, C. Chu, and M. Chen, “Hierarchical text-conditional image generation with CLIP latents,” Apr. 2022.
- [34] T. Wang, T. Zhang, B. Zhang, H. Ouyang, D. Chen, Q. Chen, and F. Wen, “Pretraining is all you need for image-to-image translation,” *arXiv preprint arXiv:2205.12952*, 2022.
- [35] S. Yang, Y. Zhou, Z. Liu, and C. C. Loy, “Rerender a video: Zero-Shot Text-Guided Video-to-Video translation,” Jun. 2023.
- [36] J. Z. Wu, Y. Ge, X. Wang, W. Lei, Y. Gu, Y. Shi, W. Hsu, Y. Shan, X. Qie, and M. Z. Shou, “Tune-A-Video: One-Shot tuning of image diffusion models for Text-to-Video generation,” Dec. 2022.
- [37] S. Yu, K. Sohn, S. Kim, and J. Shin, “Video probabilistic diffusion models in projected latent space,” Feb. 2023.
- [38] Y. He, T. Yang, Y. Zhang, Y. Shan, and Q. Chen, “Latent video diffusion models for High-Fidelity long video generation,” Nov. 2022.
- [39] N. Ruiz, Y. Li, V. Jampani, Y. Pritch, M. Rubinstein, and K. Aberman, “DreamBooth: Fine tuning Text-to-Image diffusion models for Subject-Driven generation,” Aug. 2022.
- [40] M. Hua, J. Liu, F. Ding, W. Liu, J. Wu, and Q. He, “DreamTuner: Single image is enough for Subject-Driven generation,” Dec. 2023.
- [41] Q. Wu, Y. Liu, H. Zhao, A. Kale, T. Bui, T. Yu, Z. Lin, Y. Zhang, and S. Chang, “Uncovering the disentanglement capability in text-to-image diffusion models,” pp. 1900–1910, Dec. 2022.
- [42] Q. Wang, X. Bai, H. Wang, Z. Qin, A. Chen, H. Li, X. Tang, and Y. Hu, “InstantID: Zero-shot Identity-Preserving generation in seconds,” Jan. 2024.
- [43] F. P. Papantoniou, A. Lattas, S. Moschoglou, J. Deng, B. Kainz, and S. Zafeiriou, “Arc2Face: A foundation model of human faces,” Mar. 2024.
- [44] X. Liu, D. H. Park, S. Azadi, G. Zhang, A. Chopikyan, Y. Hu, H. Shi, A. Rohrbach, and T. Darrell, “More control for free! image synthesis with semantic diffusion guidance,” in *2023 IEEE/CVF Winter Conference on Applications of Computer Vision (WACV)*. IEEE, Jan. 2023, pp. 289–299.
- [45] L. Zhang and M. Agrawala, “Adding conditional control to Text-to-Image diffusion models,” Feb. 2023.
- [46] H. Ye, J. Zhang, S. Liu, X. Han, and W. Yang, “Ip-adapter: Text compatible image prompt adapter for text-to-image diffusion models,” *arXiv preprint arXiv:2308.06721*, 2023.
- [47] A. Kumar Bhunia, S. Khan, H. Cholakkal, R. M. Anwer, J. Laaksonen, M. Shah, and F. S. Khan, “Person image synthesis via denoising diffusion model,” in *2023 IEEE/CVF Conference on Computer Vision and Pattern Recognition (CVPR)*. IEEE, Jun. 2023, pp. 5968–5976.
- [48] J. Karras, A. Holynski, T.-C. Wang, and I. Kemelmacher-Shlizerman, “DreamPose: Fashion Image-to-Video synthesis via stable diffusion,” Apr. 2023.
- [49] D. Chang, Y. Shi, Q. Gao, J. Fu, H. Xu, G. Song, Q. Yan, Y. Zhu, X. Yang, and M. Soleymani, “MagicPose: Realistic human poses and facial expressions retargeting with identity-aware diffusion,” Nov. 2023.
- [50] Z. Xu, J. Zhang, J. H. Liew, H. Yan, J.-W. Liu, C. Zhang, J. Feng, and M. Z. Shou, “MagicAnimate: Temporally consistent human image animation using diffusion model,” Nov. 2023.
- [51] X. Chen, Z. Liu, M. Chen, Y. Feng, Y. Liu, Y. Shen, and H. Zhao, “LivePhoto: Real image animation with text-guided motion control,” Dec. 2023.

- [52] T. Wang, L. Li, K. Lin, Y. Zhai, C.-C. Lin, Z. Yang, H. Zhang, Z. Liu, and L. Wang, “DisCo: Disentangled control for realistic human dance generation,” Jun. 2023.
- [53] L. Hu, X. Gao, P. Zhang, K. Sun, B. Zhang, and L. Bo, “Animate anyone: Consistent and controllable Image-to-Video synthesis for character animation,” Nov. 2023.
- [54] S. Zhu, J. L. Chen, Z. Dai, Y. Xu, X. Cao, Y. Yao, H. Zhu, and S. Zhu, “Champ: Controllable and consistent human image animation with 3D parametric guidance,” Mar. 2024.
- [55] L. Tian, Q. Wang, B. Zhang, and L. Bo, “EMO: Emote portrait alive – generating expressive portrait videos with Audio2Video diffusion model under weak conditions,” Feb. 2024.
- [56] S. Schneider, A. Baevski, R. Collobert, and M. Auli, “wav2vec: Unsupervised pre-training for speech recognition,” *arXiv preprint arXiv:1904.05862*, 2019.
- [57] E. Corona, A. Zanfir, E. G. Bazavan, N. Kolotouros, T. Alldieck, and C. Sminchisescu, “VLOGGER: Multimodal diffusion for embodied avatar synthesis,” Mar. 2024.
- [58] C. Schuhmann, R. Beaumont, R. Vencu, C. Gordon, R. Wightman, M. Cherti, T. Coombes, A. Katta, C. Mullis, M. Wortsman *et al.*, “Laion-5b: An open large-scale dataset for training next generation image-text models,” *Advances in Neural Information Processing Systems*, vol. 35, pp. 25 278–25 294, 2022.
- [59] Y. Guo, C. Yang, A. Rao, Y. Wang, Y. Qiao, D. Lin, and B. Dai, “Animatediff: Animate your personalized text-to-image diffusion models without specific tuning,” *arXiv preprint arXiv:2307.04725*, 2023.
- [60] N. Ravi, J. Reizenstein, D. Novotny, T. Gordon, W.-Y. Lo, J. Johnson, and G. Gkioxari, “Accelerating 3d deep learning with pytorch3d,” *arXiv:2007.08501*, 2020.
- [61] E. Richardson, Y. Alaluf, O. Patashnik, Y. Nitzan, Y. Azar, S. Shapiro, and D. Cohen-Or, “Encoding in style: a stylegan encoder for image-to-image translation,” in *IEEE/CVF Conference on Computer Vision and Pattern Recognition (CVPR)*, June 2021.
- [62] J. Deng, J. Guo, J. Yang, N. Xue, I. Kotsia, and S. Zafeiriou, “ArcFace: Additive angular margin loss for deep face recognition,” *IEEE Trans. Pattern Anal. Mach. Intell.*, vol. 44, no. 10, pp. 5962–5979, Oct. 2022.
- [63] J. Betker, G. Goh, L. Jing, T. Brooks, J. Wang, L. Li, L. Ouyang, J. Zhuang, J. Lee, Y. Guo *et al.*, “Improving image generation with better captions,” *Computer Science*. <https://cdn.openai.com/papers/dall-e-3.pdf>, vol. 2, no. 3, p. 8, 2023.
- [64] B. Dolhansky, J. Bitton, B. Pflaum, J. Lu, R. Howes, M. Wang, and C. C. Ferrer, “The deepfake detection challenge (dfdc) dataset,” *arXiv preprint arXiv:2006.07397*, 2020.
- [65] J. Thies, M. Zollhöfer, and M. Nießner, “Deferred neural rendering: Image synthesis using neural textures,” *Acm Transactions on Graphics (TOG)*, vol. 38, no. 4, pp. 1–12, 2019.
- [66] J. Thies, M. Zollhofer, M. Stamminger, C. Theobalt, and M. Nießner, “Face2face: Real-time face capture and reenactment of rgb videos,” in *Proceedings of the IEEE conference on computer vision and pattern recognition*, 2016, pp. 2387–2395.
- [67] S. Saha, R. Perera, S. Seneviratne, T. Malepathirana, S. Rasnayaka, D. Geethika, T. Sim, and S. Halgamuge, “Undercover deepfakes: Detecting fake segments in videos,” in *Proceedings of the IEEE/CVF International Conference on Computer Vision (ICCV) Workshops*, October 2023, pp. 415–425.
- [68] F. Chollet, “Xception: Deep learning with depthwise separable convolutions,” in *Proceedings of the IEEE conference on computer vision and pattern recognition*, 2017, pp. 1251–1258.
- [69] H. H. Nguyen, J. Yamagishi, and I. Echizen, “Capsule-forensics: Using capsule networks to detect forged images and videos,” in *ICASSP 2019-2019 IEEE international conference on acoustics, speech and signal processing (ICASSP)*. IEEE, 2019, pp. 2307–2311.

- [70] M. Tan and Q. Le, “Efficientnet: Rethinking model scaling for convolutional neural networks,” in *International conference on machine learning*. PMLR, 2019, pp. 6105–6114.
- [71] H. Dang, F. Liu, J. Stehouwer, X. Liu, and A. K. Jain, “On the detection of digital face manipulation,” in *Proceedings of the IEEE/CVF Conference on Computer Vision and Pattern Recognition (CVPR)*, June 2020.
- [72] Y. Luo, Y. Zhang, J. Yan, and W. Liu, “Generalizing face forgery detection with high-frequency features,” in *Proceedings of the IEEE/CVF Conference on Computer Vision and Pattern Recognition (CVPR)*, June 2021, pp. 16 317–16 326.
- [73] J. Cao, C. Ma, T. Yao, S. Chen, S. Ding, and X. Yang, “End-to-end reconstruction-classification learning for face forgery detection,” in *Proceedings of the IEEE/CVF Conference on Computer Vision and Pattern Recognition (CVPR)*, June 2022, pp. 4113–4122.
- [74] Y. Ni, D. Meng, C. Yu, C. Quan, D. Ren, and Y. Zhao, “Core: Consistent representation learning for face forgery detection,” in *Proceedings of the IEEE/CVF Conference on Computer Vision and Pattern Recognition (CVPR) Workshops*, June 2022, pp. 12–21.
- [75] S. Dong, J. Wang, R. Ji, J. Liang, H. Fan, and Z. Ge, “Implicit identity leakage: The stumbling block to improving deepfake detection generalization,” in *Proceedings of the IEEE/CVF Conference on Computer Vision and Pattern Recognition (CVPR)*, June 2023, pp. 3994–4004.

A Appendix / supplemental material

A.1 On deepfake detection and potential for misuse

While any face reenactment technique can also be misused for deepfake generation, it is clearly an important area of active research with many ethical applications in movies, journalism, animation and virtual reality, to name a few. This is especially apparent in emergent capabilities in techniques such as ours, as improved results in the primary domain (real human face animation) can lead to significant improvements in cross-domain or out of domain animation transfer (human to 3D, human to cartoon, cartoon to 3D, cartoon to cartoon etc.) However, to mitigate the deepfake generation potential of our approach, we perform a detailed and comprehensive analysis of state of the art detection techniques on our method, and report their zero shot performance on our data. First, this contributes to the understanding of the generalization capabilities of existing deepfake detectors. Secondly, it highlights potential for improving the training datasets of such detectors, especially with videos based on paradigms using diffusion models as the generative core. This work opens up the possibility of creating a large scale dataset of high fidelity diffusion based face reenactment videos, addressing the issue of lack of such data in the deepfake detection domain.

Deepfake Autoencoder (DFAE, e.g. DeepFaceLab²) and other face swapping methods can produce highly realistic videos that are challenging to detect using existing detection algorithms. This is evident in the results of detection algorithms on the DFDC [64] dataset. Additionally, videos generated by face reenactment methods such as Neural Texture [65] and Face2Face [66] are also difficult to detect using off-the-shelf detectors (details in [67]). It is worth noting that these methods do not offer any alternative means of detecting videos generated by them, which encourages generation of defamatory and harmful deepfakes.

Model	Frame-AUC	Video-AUC
Xception [68]	85.03	87.73
Capsule [69]	79.43	79.06
EfficientNet-B4 [70]	81.20	85.96
FFD [71]	84.79	82.59
SRM [72]	85.37	88.72
RECCE [73]	87.42	85.00
CORE [74]	89.32	87.12
CADDM [75]	86.82	95.99
Average	84.92	86.52

Table 3: Detection frame-level and video-level AUC from the state-of-the-art deepfake detectors with respective pretrained weights on videos generated by our reenactment method AniFaceDiff.

We emphasize the significance of ensuring that these methods are used ethically and that they can be detected with existing deepfake detectors; this would invalidate videos generated with malicious intent. We evaluated videos generated with our method on pretrained, state-of-the-art deepfake detection methods. Table 3 presents both frame and video-level detection results. Although video-level detection is more common, we include frame-level detection due to the possibility of temporally partial deepfakes [67] i.e. having both real and fake segments in the same video. Our evaluation encompasses multiple types of detectors including naive detectors [68, 70], a frequency-level detector [72] and spatial detectors [69, 71, 73, 74, 75]. We notice that videos generated with AniFaceDiff had high detection rate by the tested detectors. Frame-level detection is more challenging since the detection performance depends on the prediction of each frame, rather than a majority voting across the frames in a video. While the results are promising, there is room for improvement. Further investigation into diffusion-based reenactment methods could further enhance detection rates.

This assessment aims to pave the way for future studies on detection. Additionally, we provide access to researchers from deepfake detection in order to facilitate the generation of higher quality deepfake datasets, particularly those generated using state of the art face reenactment diffusion models (such as our work) - a current gap in the deepfake literature.

²<https://github.com/iperov/DeepFaceLab>

A.2 More results on cross-identity reenactment

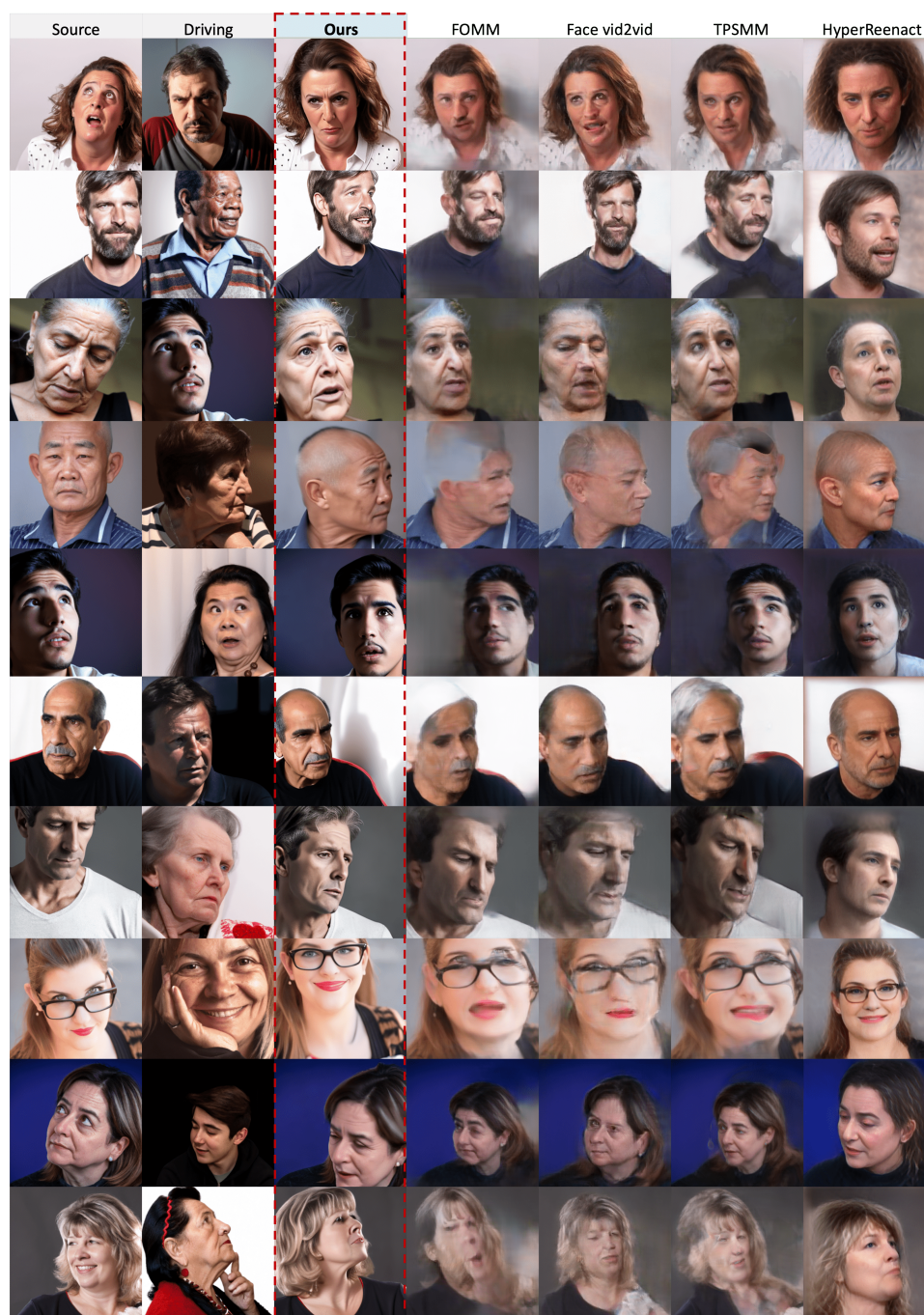


Figure 6: Additional qualitative comparison with SOTA methods on cross-identity reenactment.

A.3 More results on out-of-domain reenactment



Figure 7: Additional qualitative comparison with SOTA methods on out-of-domain reenactment.

A.4 Limitations

Although our method provides high-fidelity results with excellent image quality, there are still some limitations. First, noticeable flickering occurs when generating videos. Second, the inadvertent generation of hands affects the quality of the generated content. Future studies can focus on addressing these issues.